

Modeling of propellant combustion with nano-sized aluminum particles

Jean-Michel Lamet*, Yves Fabignon**, L. Tessé*, J. Dupays**, E. Radenac**

* *Onera – The French Aerospace Lab, F-92322, Châtillon, France*

** *Onera – The French Aerospace Lab, F-91123, Palaiseau, France*

Abstract

This paper is devoted to the analysis in combustion of two AP/HTPB composite propellants with micro-sized and nano-sized aluminum particles by using a model based on simplified gas phase, particulate phase equations and taking into account radiation field. After presenting the experimental results obtained, we estimate the minimum of aluminum particle diameter we can consider with continuum theory in gas propellant environment. We examine the modeling of aluminum particles in combustion and the modeling of radiative effects. We formulate a simple one-dimensional model to describe the combustion of aluminized propellants. This model is then used to calculate the different fluxes entering into the energetic material in order to give an explanation on physical mechanisms regarding the increasing of the burn rate due to nano-sized aluminum particles.

1. Introduction

Aluminum particles are commonly used in solid propellants to increase performance of solid rockets. It has been reported of increasing the burn rate of solid rocket propellant with addition of nano-aluminum particles. This specific behavior has been investigated by many contributors using experimental approaches. However, the cause for this burning rate increase has not been clearly identified.

Some authors [1] suggested that the characteristics of the nano-aluminum particles could store internal energy which is released during the combustion. This hypothesis was refuted by several research teams [2]. To quantify the effects of nano-aluminum particles on the propellant combustion, a recent model [3] was developed taking into account a strategy of homogenization of small particles in the binder. The combustion of nano-aluminum particles was modeled following a global approach because the physical mechanisms are not well understood at the present time. In fact, nano-aluminum particles have lower ignition temperature, faster burning rate and consequently shorter burning time due to their specific-surface area compared with micron-aluminum particles. The modeling of nano-aluminum particles in combustion in solid rocket motor remains a quite challenging task.

The purpose of this paper is to present a model to describe an AP/HTPB propellant in combustion with micro-sized and nano-sized aluminum particles. This model is based on a one-dimensional simplified approach by using gas phase and particulate phase equations. Then, radiative transfer is computed with a Monte Carlo code taking into account radiation of gaseous species and alumina droplets. We assume that there is no retrocoupling of both particulate phase and radiation field on the gas phase (weak coupling). After discussion on the hypothesis of the model in the frame of the continuum theory, we focused on the problem of modeling the combustion of nano-aluminum particles in gas propellant environment. Combustion of aluminum particles in the case of kinetically-controlled regime and diffusion-controlled regime are examined. The propellant combustion model was built following the idea developed in [4] based on low gas activation energy. The full model, including nano-aluminum particles in combustion, was then applied on two AP/HTPB composite propellants burned at ONERA. The first one contains micro-sized aluminum particles and the second bimodal nano/micro-sized aluminum particles. Results are analyzed in terms of flux entering into the energetic materials in order to give an explanation on physical mechanisms regarding the increasing of the burn rate due to nano-sized aluminum particles.

2. Results from experiments

We have considered two AP/HTPB propellants (P1 and P2) with 17% of aluminum. The total mass of AP is 68% and therefore 15% for the binder. The propellant P1 contains micro-sized aluminum particles with a mass mean diameter of 6 μm . The propellant P2 contains 20% of micro-sized aluminum particles (mass mean diameter = 6 μm) and 80 % of nano-sized aluminum particles (mass mean diameter = 100 nm). The burning rates of these propellants have been measured by using the ultrasound measurement technique [5]. At the room temperature, we have observed two different burning rate regimes (figure 1). Results show clearly the increasing of the burning rate due to nano-sized aluminum particles in the propellant. This particular behavior has been already reported by many researchers.

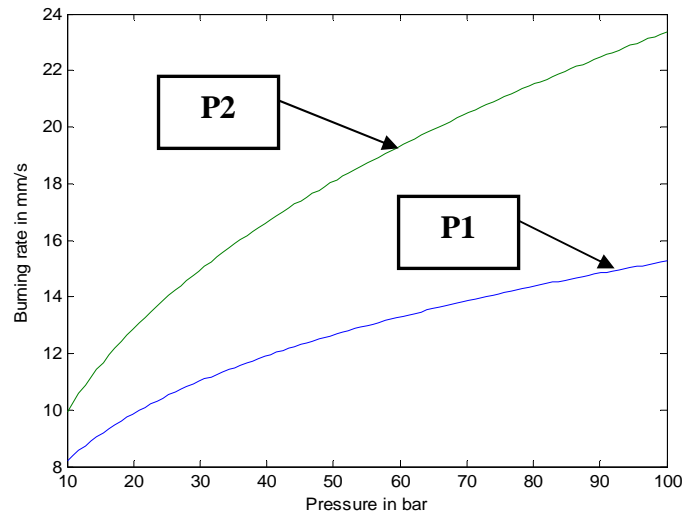


Figure 1 – Burning rate measurements for the propellants P1 and P2

3. The limit of continuum theory

In the classical approach for modeling fluid dynamics, we regard fluids as a continuous matter. For instance, Navier-Stokes equations assume the continuum hypothesis is valid (as well as the model that will be presented in sections 4 and 5). But at small length scales, the fluid must be considered as a set of discrete molecules interacting with each other, and a solution will be provided by statistical mechanics solvers. Deviation from continuum hypothesis is quantified by a Knudsen number, which is the ratio of the mean-free-path of the molecules, λ , to the characteristic length scale of the flow, L [6]:

$$Kn = \frac{\lambda}{L} = \sqrt{\frac{\pi\gamma}{2}} \frac{M}{\text{Re}} = \sqrt{\frac{\pi}{2}} \frac{rT}{PL} \frac{\mu}{PL} \quad (1)$$

γ is the ratio of specific heats for the gas. r is its specific gas constant, μ its dynamic viscosity, T its temperature and P its pressure. M is the Mach number and Re is the Reynolds number. The characteristic length scale of the flow around a droplet is the particle diameter: $L = D_p$. Some authors prefer to use the ratio M/Re instead of the Knudsen number Kn . Low-Reynolds-number flows around particles are strictly viscous (the size of the boundary layer is large compared to the size of the particle). In that case, Schaaf and Chambré [7] distinguish the four flow regimes that are displayed in figure 2. Conventional approaches are appropriate for the continuum regime: $Kn < Kn_c = 10^{-2}$. In the slip flow regime, $Kn_c < Kn < 0.14$, the droplet has significant tangential velocity and temperature drop with respect to the surrounding gas. Conventional methods are still suitable for computing such cases as long as modified conditions are used at the gas/particle interface. To perform the Direct Navier-Stokes (DNS) computation of the flow around a droplet, the boundary condition at the droplet surface must model both slip velocity and temperature discontinuity. To globally compute a two-phase flow in a Eulerian or Lagrangian way, in which gas and particle phases are coupled through a drag coefficient (momentum term) and a Nusselt number (heat transfer term), those terms must be respectively corrected by factors K_d and K_r , (see [6] for the expressions) that are plotted with respect to

Kn in figure 2. To be extensive, when the mean-free-path is comparable to the droplet size (transition regime: $0.14 < Kn < 4.11$) or larger than the droplet size (free molecule flow: $Kn > 4.11$), it is no longer possible to use continuous models, even with appropriate boundary conditions. The exact values of the Knudsen number at the boundaries between regimes are a bit arbitrary. If $Kn_c = 10^{-2}$, as suggested by Schaaf and Chambré, the continuous drag coefficient and Nusselt numbers are accurate to less than 3%: in the continuous regime, K_d and K_t are always in the range $[0.97; 1]$. According to Devienne [8], $Kn_c = 10^{-3}$, which may be a consequence of a smaller accuracy tolerance than the one of Schaaf and Chambré. For an extended range of validity such that a 15% relative error in drag and heat flux is permitted, $Kn_c = 5 \cdot 10^{-2}$.

To give some practical information in the case of this study, let us consider a propellant gas in which aluminum droplets burn. Equilibrium calculations at $P=50$ bar give a temperature $T \approx 3600$ K and $\mu = 9 \cdot 10^{-5}$ kg.s⁻¹.m⁻¹, $\gamma = 1.2$, $M \approx 0.029$ kg/mol. In that case, $Kn = 1$ if the diameter of aluminum droplets is 23 nm. If the boundary between continuous and slip flow regimes is $Kn_c = 10^{-2}$, the smallest particle size that can be computed by a genuine conventional approach is 2.3 μ m. With Devienne's very strict conception of continuum, the minimum diameter would be 23 μ m ! On the contrary, if $Kn_c = 5 \cdot 10^{-2}$, the use of continuous approaches is extended to particles larger than 460 nm. However, it must be noted that the boundaries between regimes were defined for inert droplets. In solid propellant rockets, the combustion of aluminum droplets changes both heat transfer and drag, which may affect the different thresholds depicted in figure 2. Due to this uncertainty, we have considered $K_d = K_t = 1$ in our first model.

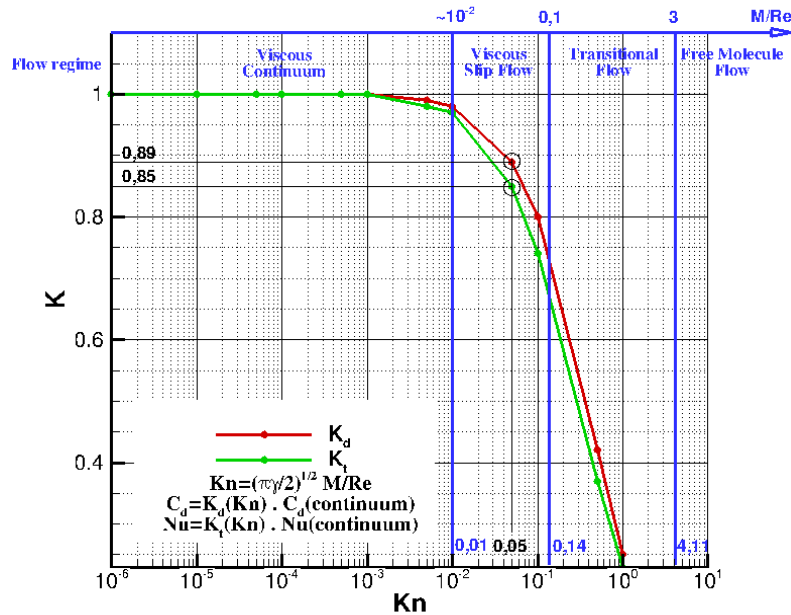


Figure 2 –Momentum and heat transfer correcting factors K_d and K_t as function of Knudsen number

4. Modeling of nano-aluminum particles in combustion

The modeling of the particle combustion will depend on different length or time scales as the particle size, the mean free path of the surrounding gas-phase, the mass and energy transport time scales, and the chemical time scale. Other parameters are important to determine if the combustion will occur either heterogeneously at the particle surface or homogeneously in the surrounding gas phase.

In the first case, the surface reaction is assumed to follow the global chemical equation $\nu'_F F + \nu'_O O \rightarrow \nu''_P P$ or, in term of masses, $F + sO \rightarrow (1 + s)P$ between the oxidizer molecules O as CO_2 and H_2O , and the fuel F, i.e. the aluminum in the liquid phase. The reaction leads to the combustion products P that contain both gas molecules and condensed aluminum oxide smokes. The coefficients ν'_F , ν'_O , ν''_P and s are the molar and mass stoichiometric coefficients of the reaction. At this stage, an important assumption, that should be checked, is made to derive the aluminum surface reaction rate. The oxidizer and product molecules are assumed to be weakly adsorbed on the surface so that, following the Langmuir adsorption isotherm model, the surface reaction is first-order with respect to the oxidizer [9], [10]; The reaction rate is proportional to the gas-phase concentration of the oxidizer adjacent to the surface and the aluminum reaction rate is simply:

$$\dot{W}_F^\sigma = -\nu'_F M_F k^\sigma(T_s) C_{O,s}^+ = -\nu'_F M_F k^\sigma(T_s) \frac{P}{R_u T_s} X_{O,s}^+ \quad (2)$$

where $C_{O,s}^+$ and $X_{O,s}^+$ are the molar concentration and the molar fraction of oxidizer at the surface, M_F the molecular weight of the fuel, R_u the universal gas constant, T_s the surface temperature and $k^\sigma(T_s)$ the rate coefficient, which depends on the surface temperature through an Arrhenius form, i.e. $k^\sigma(T_s) = A^\sigma \exp(-E_a^\sigma/R_u T_s)$. If θ is the fraction of the particle surface covered by adsorption then the aluminum mass flow rate from the particle is:

$$\dot{m} = \theta \pi d^2 \nu'_F M_F k^\sigma \frac{P}{R_u T_s} X_{O,s}^+ \quad (3)$$

The fraction θ is usually less than 1 because of the presence of a non porous oxide cap on the particle and is a non trivial function of the particle diameter. This complex dependence precludes from deriving a general analytic expression for the particle combustion time. However, with no oxide cap, the combustion time for a particle of initial diameter d_0 and density ρ_F is simply:

$$\tau_{kin} = \frac{d_0 \rho_F R_u T_s}{2 \nu'_F M_F k^\sigma P X_{O,s}^+} \quad (4)$$

Thus, the particle combustion follows theoretically a $d^{1.0}$ law in a kinetically-controlled regime compared to a $d^{2.0}$ law in a diffusion-controlled regime with:

$$\tau_{diff} = \frac{\rho_F d_0^2}{8 \rho D \ln(1+B)} \quad (5)$$

where D is the mass diffusivity which is proportional to P^{-1} . The expression for B will depend on the position of the reaction zone [11]. The comparison between these two characteristic times shows that the pressure and the particle size are important parameters to determine the combustion regime: large particles at high pressure likely experience diffusion-controlled combustion while small particles at low pressure likely experience kinetically-controlled combustion.

Numerous experiments and simulations at the particle level were conducted to determine the combustion law followed by aluminum particles, including at ONERA [12]. The compilation provided by Beckstead for micron and larger-sized particles [13] led him to build an empirical correlation, commonly used today, based on a $d^{1.8}$ law that supports the argument of a combustion driven by diffusion mechanisms. The combustion time is given by:

$$\tau_c = \frac{d_0^{1.8}}{k_c X_{eff} P^{0.1} T^{0.2}} \quad (6)$$

where $X_{eff} = X_{O_2} + 0.6 X_{H_2O} + 0.22 X_{CO_2}$ is the effective oxidizer mole fraction and k_c a constant equal to $6,265 \cdot 10^{-7}$ in standard units.

For smaller particles, and nano-sized particles in particular, information is more limited. Huang et al. [14] reported interesting results for nano-sized particles and compare them with some classical results for larger particles. The compilation is shown on the figure 3 (from ref [14]) that reproduces the measured particle burning time as a function of particle size. The combustion of smaller particles follows a very different law as expected but with a 0,3 exponent instead of a 1,0 exponent. In spite of the efforts to maximize particle dispersion in the burner, the possible occurrence of particle agglomeration was suggested by the authors to explain the deviation. But, other explanations, perhaps of secondary importance, can also be suggested. For instance, as mentioned above, the validity of the $d^{1.0}$ law must be questioned with the presence of an oxide cap that can noticeably limit the adsorption surface and introduce a complex diameter dependence.

Whatever the exponent value is, a limit size separating the two regimes can be deduced from these data. For chamber conditions with high temperature, the limit seems to be about a few microns. This result can be used to determine the rate coefficient of the surface reaction, when assuming a $d^{1.0}$ law for smaller particles, by simply equalize, for this limit size, the burning time in the kinetic regime with the burning time given by the Beckstead's correlation. The kinetic combustion model was then introduced in our code to determine the thickness η_{Al} of the distributed combustion zone of aluminum particles above the propellant surface. In this model, the acceleration of the particles is due to the drag force only. The inverse coupling of the particles on the gas was not considered. Finally, results from this model can be interpreted with the following equation:

$$\eta_{Al} = k d_0^n \quad (7)$$

where k and n depend on the regime considered for the combustion of aluminum particles. It can be mentioned that combustion zone is thicker when applying the $d^{1.0}$ law, as expected. The deviation between the results given by the two different laws can be dramatically high for nano-sized particles. For instance, the thickness is hundred times wider for 100 nm diameter particles when applying the $d^{1.0}$ law instead of the $d^{1.8}$ law. The correlation between the particle diameter and the thickness of the combustion zone was then used to evaluate the heat flux profile and the radiant heat feedback to the propellant surface.

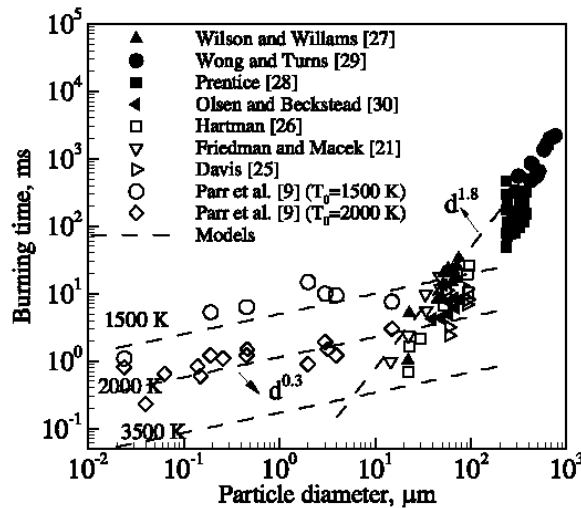


Figure 3 – Aluminum particle burning time as function of particle diameter (from ref [14]).

5. Modeling of the combustion of aluminized propellants

The objective is to develop a predictive engineering model of combustion of aluminized propellants. We assume a one-dimensional steady state approach of the problem. We also consider a weak coupling that means no retrocoupling of both particulate phase and radiation field on the gas phase. According to the references [4] and [15], with the assumption of constant gas properties and low activation energy in the reaction zone, the temperature and species profiles between the propellant surface (s) and the flame (f) are:

$$\frac{T(\eta) - T_f}{T_s - T_f} = \frac{Y(\eta)}{Y_s} = \exp(-\nu_2 \frac{\eta}{\eta_f}) \quad (8)$$

η is the coordinate normal to the propellant surface and η_f the flame location. ν_2 is the thermal wave thickness for which the temperature is at 90 % of its final value. The flame location is given by an energy balance between $\eta = 0$ and $\eta = \eta_f$. Using these simple considerations, we can build a model including aluminum particles in combustion. Figure 4 shows a schematic diagram of temperature profile for aluminized propellants in combustion. The coordinate

$\eta = 0$ is defined as the gas/solid interface in regression. With this description, zone 1 corresponds to the solid phase. The surface temperature T_s is determined by using experimental results on the pyrolysis law of the propellant considered. It is generally written as:

$$V_c = A_p \exp(-E_p / R_u T_s) \quad (9)$$

where V_c is the burning rate, A_p the pre-exponential factor, and E_p the activation energy. Zone 2 is devoted to the combustion due to the gas phase reactions. Aluminum particles are transported until the coordinate $\eta = \eta_{ign}$ where ignition occurs. Zone 3 corresponds to the distributed combustion of aluminum particles. The temperature and species profiles between $\eta = \eta_{ign}$ and the final flame $\eta = \eta_{Al}$ are:

$$\frac{T(\eta) - T_{f,Al}}{T_{ign} - T_{f,Al}} = \frac{Y_{Al}}{Y_{Al,f}} = \exp\left[-v_3 \frac{(\eta - \eta_{ign})}{(\eta_{Al} - \eta_{ign})}\right] \quad (10)$$

According to the reference [16], the ignition temperature of aluminum particle is a function of particle diameter. The final temperature $T_{f,Al}$ is obtained for $\eta = \eta_{Al}$ given by equation (7).

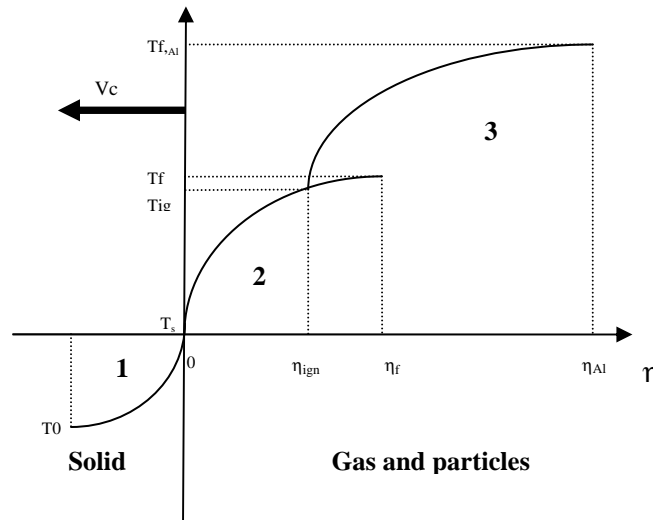


Figure 4 – Schematic of temperature profile for the combustion model

With this model and propellant data, it is possible to get temperatures T_f and $T_{f,Al}$ by using equilibrium calculations and finally temperature profiles with equations (8) and (10). Fluxes are also known by derivating equations (8) and (10). Equilibrium calculations provide also species for coordinates η_f and η_{Al} . For AP/HTPB composite propellant, we have considered only six species (Al_2O_3 (l), CO, CO_2 , H_2O , HCl, N_2). Species profiles are then computed with equations (8) and (10) to determine the gas environment for aluminum particles in combustion and radiative calculations. It is important to underline with this model that we can only get the mass fraction of alumina for the aluminum combustion zone 3. No information is known regarding the size of alumina residue which is an input parameter.

6. Modeling of radiative transfer

In this study, radiative transfer computations have been carried out in post processing in order to evaluate the radiative flux incident on the propellant surface. There is no coupling between combustion and radiative transfer: radiative powers have not been used in the one-dimensional combustion modeling.

Radiative transfer computations have been performed using a 3D Monte Carlo method [17-19]. This approach consists in following a finite large number of energy bundles (discrete amounts of energy, which can be pictured as a group of photons bound together) throughout their transport histories, from emission to absorption. Bundle characteristics, namely wave number, initial direction and emission point, and physical events (scattering, reflection off walls... except absorption) along bundle trajectories are chosen according to probability distributions by drawing random numbers. Absorption phenomenon is treated with the pathlength method [20], also called energy partitioning [21], which consists in computing exponential absorption along the path. Therefore, a bundle contributes to every cell it traverses. It is traced until it either leaves the computational domain or until its energy is depleted below a given cut-off level. Since all the bundles are statistically independent, the parallelization is achieved by distributing them over the cores.

Gas radiative properties are modeled by using a Statistical Narrow-Band (SNB) model in the weak absorption approximation since pressure considered in this study is high (50 bar). Under this assumption, the band averaged transmissivity $\bar{\tau}^{\Delta\nu}$ of a column of length ℓ writes:

$$\bar{\tau}^{\Delta\nu} \approx \prod_{i=1}^{N_{as}} \exp\left(-\int_0^{\ell} x_i(s) p(s) \bar{k}_i^{\Delta\nu}(s) ds\right) = \exp\left(-\int_0^{\ell} p(s) \sum_{i=1}^{N_{as}} x_i(s) \bar{k}_i^{\Delta\nu}(s) ds\right) \quad (11)$$

where N_{as} is the number of gaseous absorbing species, x_i the molar fraction of the species i , p the total pressure and $\bar{k}_i^{\Delta\nu}$ the reduced absorption coefficient of the species i , a parameter of the SNB model. According to equation (11), the local absorption coefficient $\bar{K}^{\Delta\nu}$ can be expressed as:

$$\bar{K}^{\Delta\nu}(s) \approx p(s) \sum_{i=1}^{N_{as}} x_i(s) \bar{k}_i^{\Delta\nu}(s) \quad (12)$$

In this study, four gaseous absorbing species have been considered: CO₂, H₂O, CO and HCl. To compute absorption coefficients of this gaseous mixture, the parameters generated by Duval et al. [22] have been used. These parameters have been tabulated for 43 spectral bands in the infrared spectral range (1 μm – 73 μm) and for 14 temperatures between 300 K and 2900 K. For upper temperatures, parameters at 2900 K have been used.

Concerning the particles, only alumina droplets have been considered in this study. In first approximation, aluminum particles have not been taken into account in radiative transfer calculations. Alumina droplets are assumed to be spherical, homogeneous and isothermal. Then Mie theory is applied to compute radiative properties: absorption and scattering coefficients and phase function. The alumina complex refractive index m is modeled as a function of wavelength λ and temperature T in accordance with the expression given by Dombrovsky [23] such as:

$$m_{\lambda}(T) = n_{\lambda}(T) + i\chi_{\lambda}(T) \quad (13)$$

with the following expressions for the refractive index n , and the absorption index χ :

$$n_{\lambda}(T) = \left[1 + \lambda^2 \left(\frac{1.024}{\lambda^2 - 3.776 \times 10^{-3}} + \frac{1.058}{\lambda^2 - 1.225 \times 10^{-2}} + \frac{5.281}{\lambda^2 - 321.4} + \right) \right]^{0.5} \times [1 + 2.02 \times 10^{-5} (T - 473.0)] \quad (14)$$

$$\chi_\lambda(T) = 2.0 \times 10^{-3} (1 + 0.7\lambda + 0.06\lambda^2) \exp[1.847 \times 10^{-3} (T - 2950)] \quad (15)$$

where λ is expressed in μm . Alumina droplets are considered to be at thermal equilibrium with the gases. Particle size distribution is approximated by a Gaussian function with a standard deviation equal to 10 % of the mean diameter. Several values of the mean diameter have been tested. Results are presented in the next Section.

7. Results

We have considered two AP/HTPB composite propellants as described in section 2. The chamber pressure is 50 bar. For this pressure, equation (9) allows to get the surface temperature of the two propellants through experimental burning rates. A simple steady conductive heat transfer in the solid (zone 1, figure 1) gives the heat flux entering into the energetic material. Table 1 below shows results obtained for the two propellants.

Table 1: Burning rate, surface temperature and flux entering into the energetic materials at $p = 50$ bar

	Propellant P1	Propellant P2
Burning rate	12,6 mm/s	18 mm/s
Surface temperature	980 K	1020 K
Flux entering into the material	19 MW/m ²	29 MW/m ²

Computations have been carried out separately for gas phase, particulate phase and radiative transfer because no retrocoupling of both particulate phase and radiation field on the gas phase has been considered. Equilibrium calculations provide parameters for gas phase in terms of boundary temperature and species. The present model then returns temperature and species profiles above the propellant surface. For the propellant P1, the aluminum particle diameter is 6 μm . For the propellant P2, the average aluminum particle diameter is 100 nm. For these two propellants, we did not consider agglomeration of aluminum particles on the surface. If we assume a combustion of aluminum particles driven by diffusion mechanisms, propellant P2 gives a very short ($\eta_{\text{Al}} = 0.42 \mu\text{m}$) distributed combustion region. This result is probably not plausible. With the assumption of combustion driven by kinetic mechanisms, the distributed combustion region is hundred times wider. Table 2 summarizes the main parameters used in the calculations.

Table 2: Main parameters used in the calculations

	Propellant P1	Propellant P2	
Flame temperature T_f without aluminum	2317 K	2317 K	
Flame temperature $T_{f,\text{Al}}$ with aluminum combustion	3384 K	3384 K	
Mean aluminum particle diameter dp_0	6 μm	100 nm	100 nm
Combustion regime of Al particles	diffusion	diffusion	kinetic
k in equation (7)	16.5	22	403
n in equation (7)	1.7	1.72	0.97
Ignition temperature of Al particles	2050 K	1300 K	
Distributed combustion length scale η_{Al}	347 μm	0.42 μm	43.1 μm

Figure 5 shows temperature and volume fraction of alumina droplets profiles above the surface for propellants P1 and P2. It is clear that, for the chamber pressure considered, propellant P2, with nano-sized of aluminum particles, gives a stiff temperature profile. The full combustion region is roughly 50 μm for the propellant P2 and 500 μm for the propellant P1. The last line of the table 2 shows results.

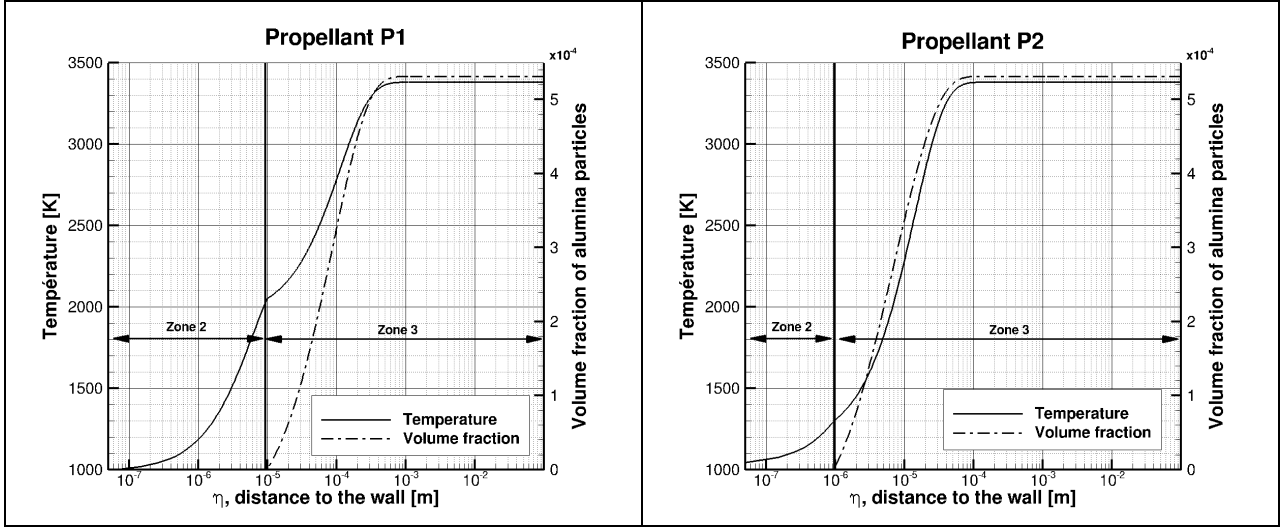


Figure 5: Temperature and volume fraction of alumina droplets profiles obtained above the propellant surface

From one-dimensional thermo-chemical profiles (temperature, mass fractions of species and volume fractions of alumina droplets) obtained previously, radiative calculations have been performed. Beforehand, one-dimensional profiles have been projected on a three-dimensional box (configuration similar to tangent slab method). The propellant surface is considered as an opaque body characterized by an isotropic emissivity $\varepsilon = 0.9$ and a surface temperature $T_s = 980$ K for P1 and $T_s = 1020$ K for P2 (see table 1).

Without experimental or numerical results on alumina droplet size (this depends on complex phenomena such as aluminum agglomeration on the propellant surface, aluminum combustion and alumina coalescence in the flame), simulations have been performed with different diameters $d_{Al_2O_3}$ of alumina droplets ($1 \mu\text{m}$ and $10 \mu\text{m}$) for the two propellants. This allows estimating the droplet size sensitivity of the radiative flux. Figure 6 shows the computing results in terms of radiative flux incident to the surface. All results show medium is optically thick beyond a distance η_{thick} to the propellant surface. The incident radiation from this zone corresponds to the black body radiation at the temperature of the medium ($T = 3384$ K for both propellants):

$$\Phi_{incident}^{rad}(\eta_{thick}) = \sigma T^4 = 7,43 \text{ MW} / \text{m}^2, \quad (16)$$

where σ is the Stephan-Boltzmann constant. Close to the surface, for $\eta < \eta_{thick}$, the incident flux decreases due to the presence of the propellant. The distance η_{thick} is similar for the two propellants P1 and P2 and depends on the droplet diameter: $\eta_{thick} \approx 1$ cm for $d_{Al_2O_3} = 1 \mu\text{m}$ and $\eta_{thick} \approx 4$ cm for $d_{Al_2O_3} = 10 \mu\text{m}$. To explain this difference, table 3 shows radiative properties of the alumina droplets at thermophysical conditions for $\eta > \eta_{Al}$ ($T = 3384$ K and volume fraction $f_{v,Al_2O_3} = 5,32 \cdot 10^{-4}$ for the two propellants) and for the spectral band centered at the wavenumber 6630 cm^{-1} (this wavenumber corresponds to the maximum of the Planck function at 3384 K). Firstly, we note that, whatever particle size, the scattering coefficient is larger than absorption coefficient, which indicates that radiative transfer is mainly governed by scattering phenomenon. Secondly, scattering coefficient for $d_{Al_2O_3} = 1 \mu\text{m}$ is 14 times larger than the one for $d_{Al_2O_3} = 10 \mu\text{m}$. The medium is optically thicker (by scattering) in the case of alumina droplets of $1 \mu\text{m}$ that is the reason why the decrease of the flux (due to the attenuation of the backscattering) occurs closer to the propellant surface compared to the cases with larger droplets. For the same reason, the attenuation of the incident radiative flux is more important above the surface in the case of $d_{Al_2O_3} = 1 \mu\text{m}$. The radiation received by the surface is thus highly dependent on the size of the alumina droplets.

Table 3: Radiative properties of the alumina droplets at 6630 cm⁻¹

Particle diameter [μm]	Absorption coefficient [cm^{-1}]	Scattering coefficient [cm^{-1}]
1	1	35
10	0,3	2,5

In addition, Figure 6 shows propellant P2 generates a slightly larger flux compared to the one generates by propellant P1 for the same alumina diameter. This is because in the case of propellant P2, the flame front is much closer to the wall which reduces the extinction phenomenon and increases backscattering effect.

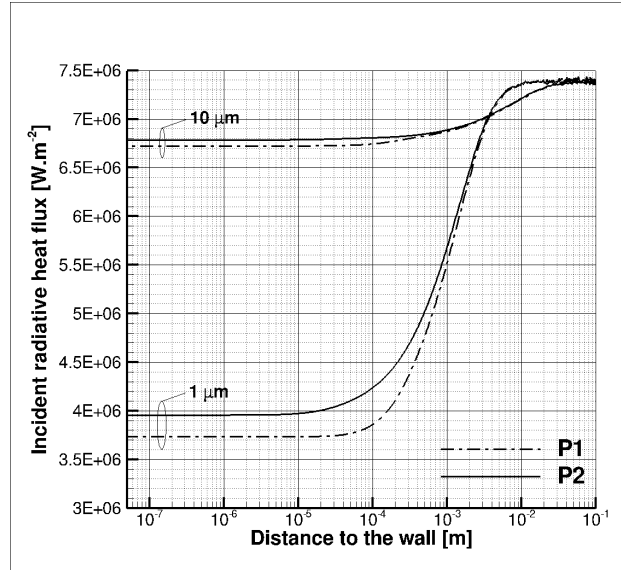


Figure 6: Incident radiative heat flux as function of distance to the burning surface

From these results, the net radiative flux to the propellant surface can be deduced from the following expression:

$$\Phi_{net}^{rad} = \varepsilon(\Phi_{incident}^{rad} - \sigma T_s^4). \quad (17)$$

Moreover, the incoming heat flux Φ^{in} to the propellant surface is the sum of the convective-conductive and net radiative flux minus the heat flux Φ^p required for the pyrolysis of the propellant:

$$\Phi^{in} = \Phi^{cc} + \Phi_{net}^{rad} - \Phi^p = \Phi^{tot} - \Phi^p. \quad (18)$$

Considering thermo-physical properties of the propellants, we have obtained $\Phi^p = 6,18 \text{ MW/m}^2$ for P1 and $\Phi^p = 8,83 \text{ MW/m}^2$ for P2. With these values and values of Φ^{in} given in the table 1 ($\Phi^{in} = 19 \text{ MW/m}^2$ for P1 and $\Phi^{in} = 29 \text{ MW/m}^2$ for P2), we can deduce from relation (17) and (18) the contribution of the radiative flux and the convective-conductive flux to the total flux on the propellant surface for the two alumina droplet diameters. The results are summarized in Table 4. For propellant P1, convective-conductive and radiative fluxes contribute respectively to 87% and 13% of the total flux in the case of $d_{Al_2O_3} = 1 \mu\text{m}$ (76 % and 24 % in the case of $d_{Al_2O_3} = 10 \mu\text{m}$). The radiative flux is even more important when alumina droplet diameter is large. For propellant P2, the tendency is similar but the contribution of the convective-conductive flux is larger (84-91%). In fact, in comparison to result for propellant P1, propellant P2 generates a higher radiative flux (3 to 7% more) for the same alumina droplet diameter, but the proportion of the radiative flux to the total flux decreases. Consequently, the increase of the heat flux received by the surface of the propellant P2 (and thus the increase of burning rate) is mainly due to the increase (57-65%) of the convective-conductive flux. In terms of total fluxes, these results show an increase of 50% between propellants P1 and P2.

Table 4: Convective-conductive and radiative heat fluxes on the propellant surface

Alumina droplet diameter	Propellant	Convective-conduction		Radiation	
		Convective-conductive flux [MW/m ²]	Contribution to the total flux	Radiative flux [MW/m ²]	Contribution to the total flux
1 μm	P1	21,9	87%	3,3	13%
	P2	34,3	91%	3,5	9%
10 μm	P1	19,2	76%	6	24%
	P2	31,7	84%	6,1	16%

8. Conclusions

The work we have carried out in this paper concerns the modeling of AP/HTPB composite propellant in combustion with micro-sized and nano-sized aluminum particles. The one-dimensional steady state model used for the calculations is based on a low gas activation energy approximation, aluminum particles in combustion and a determination of radiative fluxes taking into account alumina and four gaseous species. For the modeling of aluminum particles in combustion, we have considered a kinetics-controlled regime or a diffusion-controlled regime. Gas phase, particulate phase and radiative effects have not been coupled in this first work. We have assumed that there is no retrocoupling of both particulate phase and radiation field on the gas phase (weak coupling). According to the first calculations in the frame of continuum theory for gas propellant environment, the smallest inert particle size of aluminum that can be computed by a genuine conventional approach is 2.3 μm . If smaller particles are considered, we need to add a correction K_d in drag coefficient and a correction K_r in Nusselt number. However, we did not find any results regarding these corrections for aluminum particles in combustion. Therefore, in our first approach presented here, we have used no corrections for K_d and K_r . It is clear those values must be re-estimated in a future work.

Calculations using this first model have been carried out on two AP/HTPB propellants with micro-sized aluminum particles (6 μm) and nano-sized aluminum particles (100 nm). Results showed the important effect of the aluminum particle diameter on the temperature profiles. Radiative transfer calculations have been carried out with different alumina droplet diameters. For the same alumina droplet diameter, results show that radiative heat flux increases slightly in the case of propellant with nano-sized aluminum particles. Results on radiative and convective-conductive fluxes on the propellant surface shows the increase of the total heat flux in the case of propellant with nano-sized particles. If no chemical reactions with nano-sized aluminum particles are considered on the propellant surface, the increase of the burn rate is mainly due to the increase of the convective-conductive flux.

To improve this first approach, future works will consist in modeling combustion with polydispersed aluminum particles and taking into account radiative properties of aluminum particles in radiation calculations.

Acknowledgment

This work was supported by the Délégation Générale de l'Armement from the French Ministry of Defence.

References

- [1] Ivanov, G., and F. Tepper. 1997. Activated aluminum as a stored energy source for propellants. *Challenges in Propellants and Combustion 100 years after Nobel*. Edited by K. Kuo et al, Begell House, New York. pp 636-645.
- [2] Mench, M., C. Yeh, and K. Kuo. 1998. Propellant burning rate enhancement and thermal behavior of ultra-fine aluminum powders (ALEX). *Energetic materials production, processing and characterization*. Fraunhofer Institut Chemische Technologie, Karlsruhe. Germany. pp 30-1-30-15.
- [3] Jackson, T. L., J. Buckmaster, and W. Wang. 2007. Modeling of propellants containing ultra fine aluminum. *Journal of Propulsion and Power* 23:158-164.
- [4] Lengelle, G., J. Duterque, and J.-F. Trubert. 2000. Physico-chemical mechanisms of solid propellant combustion. *Progress in Astronautics and Aeronautics* 185:287-334.

- [5] Cauty, F. 2000. Ultrasonic method applied to full-scale solid rocket motors. *Journal of Propulsion and Power* 16:523-528.
- [6] Clift, R., J. R. Grace, and M. E. Weber. 1978. Bubbles, Drops and Particles. *Academic Press*.
- [7] Schaaf, S.A., and P. L. Chambré. 1958. Fundamentals of Gas Dynamics. Section H: Flow of rarefied gases. *Princeton University Press*.
- [8] Devienne, F. M. 1958. Frottement et échanges thermiques dans les gaz raréfiés. *Gauthier-Villars Editeur*.
- [9] Gardiner, W. C. Jr. 1969. Rates and mechanisms of chemical reactions. *W. A. Benjamin, Inc.*
- [10] Upadhyay, S. K. 2006. Chemical kinetics and reaction dynamics. *Springer*.
- [11] Turns, S. R. 2000. An introduction to combustion, concepts and applications, *Second edition, McGraw Hill*.
- [12] Dupays, J., Y. Fabignon, O. Orlandi and J.-F. Trubert. 2000. Combustion of aluminum particles in solid rocket motors. *2nd ONERA-DLR Aerospace Symposium*, Berlin, Germany, June 15-16.
- [13] Beckstead, M. W. 2002. A summary of aluminum combustion, *RTO/VKI Special Course on Internal Aerodynamics in Solid Rocket Propulsion, Von Karman Institute for Fluid Dynamics, RTO-EN-023, May*.
- [14] Huang, Y., G. A. Risha, V. Yang, and R. A. Yetter. 2007. Combustion of bimodal nano/micron-sized aluminum particle dust in air. *Proceedings of the Combustion Institute* 31:2001-2009.
- [15] Brewster, M. Q., M. J. Ward, and S. F. Son. 1997. New paradigm for simplified combustion modeling of energetic solids: branched chain gas reaction. *AIAA paper 97-333, 33rd AIAA/ASME, SAE/ASEE Joint propulsion conference & exhibit*.
- [16] Trunov, M. A., M. Schoenitz, and E. L. Dreizin. 2005. Ignition of aluminum powders under different experimental conditions. *Propellants, Explosives, Pyrotechnics* 30:36-43.
- [17] Tessé, L., and J.-M. Lamet. 2011. Radiative transfer modeling developed at Onera for numerical simulations of reactive flows. *AerospaceLab Journal*, Issue 2. <http://www.aerospacelab-journal.org/al2>
- [18] Rouzaud, O., L. Tessé, T. Soubrié, A. Soufiani, Ph. Rivière, and D. Zeitoun. 2008. Influence of radiative heating on a Martian orbiter. *Journal of Thermophysics and Heat Transfer* 22:10-19.
- [19] Tessé, L., F. Dupoirieux, and J. Taine. 2004. Monte Carlo modeling of radiative transfer in a turbulent sooty flame. *International Journal of Heat and Mass Transfer* 47:555-572.
- [20] Farmer, J. T., and J. R. Howell. 1998. Comparison of Monte Carlo strategies for radiative transfer in participating media. *Advances in Heat Transfer* 31:333-429.
- [21] Modest, M. F. 2003. Radiative heat transfer. 2nd edition, Academic Press, San Diego, CA, USA.
- [22] Duval, R., A. Soufiani, and J. Taine. 2004. Coupled radiation and turbulent multiphase flow in an aluminized solid propellant rocket engine. *Journal of Quantitative Spectroscopy and Radiative Transfer* 84:513-526.
- [23] Dombrovsky, L. A. 1982. Possibility of determining the disperse composition of a two-phase flow from the small-angle light scattering. *High Temp.* 20:472-479.